Article

Not peer-reviewed version

Investigation of Anti-Cancer Properties of Novel Curcuminoids in Leukemic Cells and Dalton Lymphoma Ascites Model

Subhas S Karki *, Vijayalakshmi Sudarshan, P Shyamjith, Sujeet Kumar, Bibha Choudhary, Febina Ravindran

Posted Date: 23 January 2025

doi: 10.20944/preprints202501.1735.v1

Keywords: curcuminoids; leukemia; cyclopentanone derivatives; monoketone; cytotoxicity; apoptosis

Article

Investigation of Anti-Cancer Properties of Novel Curcuminoids in Leukemic Cells and Dalton Lymphoma Ascites Model

Vijayalakshmi S [1], Shyamjith P [2], Sujeet Kumar [1], Febina Ravindran [2],Subhas S Karki [1,*] and Bibha Choudhary [2,*]

[1] Dept of Pharmaceutical Chemistry, KLE College of Pharmacy, Rajajinagar, Bengaluru 560010, Karnataka, India

[2] Institute of Bioinformatics and Applied Biotechnology, Electronic City Phase 1, Bengaluru 560100, Karnataka, India

* Correspondence: subhasskarki@gmail.com (Subhas S Karki); vibha@ibab.ac.in (Bibha Choudhary)

Abstract: Leukemia, one of the major causes of cancer death, ranks 11th worldwide among cancer-related deaths. The current treatment of leukemia faces challenges recently due to a high burden of side effects. It is well established that curcumin has anticancer and tumor-suppressing activities in several cancers in addition to leukemia. Accordingly, 15 derivatives were designed, prepared and evaluated for their cytotoxicity against the leukemic cell line MOLT-4, which led to the prioritization and further evaluation of compound **5i**. Compared to curcumin, **5i** was significantly more effective in inducing mitochondrial dysfunction in MOLT-4 cells; hence increased ROS production and cytotoxicity. Treatment groups showed translocation of mitochondrial membrane potential by flow cytometry analysis. Moreover, tumor volume reduction observed with **5i** treatment in Dalton's Lymphoma model was with rather low toxicity signs. Intrinsic pathways of apoptosis were initiated by compound **5i** that lowered Bcl-2 expression statically while augmenting cytochrome c levels both *in vivo* and *in vitro*. These results showcase the potent antiproliferative and cytotoxic effects of **5i** at nanomolar doses against leukemia, at least 60X better than curcumin.

Keywords: curcuminoids; leukemia; cyclopentanone derivatives; monoketone; cytotoxicity; apoptosis

1. Introduction

Leukemia is one type of cancer that involves uncontrollable production as well as accumulation of blast or immature atypical blood cells in bone marrow and peripheral blood. It ranks among the top ten cancers diagnosed globally [1]. Approximately 3.4% of cancer-related deaths worldwide in 2022 were attributed to leukemia [2]. Although it can affect individuals at any age, most cases are diagnosed among children and older adults [3]. The cause of leukemia is not fully established; however, it is believed to be a combination of genetic and environmental factors or both [4]. Conventional treatments for cancer, such as chemotherapy, radiotherapy, and surgical excision, are inadequate; therefore, to gain control over this complicated milieu, one must resort to therapies possessing site-specific characteristics and few side effects on normal tissue as well as methods that prevent metastasis [5]. New strategies used in the treatment of cancer include apoptosis induction, gene expression alteration, and signal transduction pathway inhibition. Apoptosis induction allows the cancer cells' death selectively without affecting the normal ones. This can be achieved by altering the level of particular proteins responsible for apoptosis regulation such as BAX, Bcl-2, caspase-3, caspase-9, tubulin and various kinases. The enhancement of apoptotic cell death is correlated with upregulation of pro-apoptotic proteins BAX or downregulation of anti-apoptotic protein Bcl-2. Caspases which constitute a proteolytic enzyme family fosters apoptosis development greatly and

 doi:10.20944/preprints202501.1735.v1

initiator caspases like caspase-9 and effector or apoptotic caspase-3 are strongly imperative to the progression of apoptosis [6].

Exploration and development of the drugs from the secondary metabolites obtained from the medicinal plants have always been the base in searching for anticancer agents and in this regard, much interest has been drawn towards curcumin, a linear diarylheptanoid natural product that contains two oxygen-substituted aryl groups connected by a seven-carbon chain [7]. This phytochemical exhibits a wide range of biological activities, such as antiarthritis, antiatherosclerosis, antibacterial, antidiabetic, antifungal, antihypertensive, antihyperlipidemic, anti-inflammatory, antitumor, antiphlogistic, antipsoriatic, antithrombotic, and antihepatotoxic properties [8]. It has also shown significant cytotoxic effect and caused cell death in different leukemic cell lines and downregulated the WT1 and FLT3 protein expressions related to cell proliferation [1]. It exerts its anticancer activity by inhibiting key biological pathways such as mutagenesis, oncogene expression, cell cycle regulation, tumor progression, and metastasis. It also modulates signaling pathways, enhances tumour suppressor proteins (p53, p21, p27), and promotes apoptosis by reducing pro-survival gene products.

Moreover, curcumin is very effective as an anticancer agent by inhibiting several biological pathways like mutagenesis, oncogene expression, cell cycle regulation, tumor development, and metastasis [9]. Studies have shown that curcumin regulates many signaling pathways in cells, increases the levels of tumor suppressor proteins p53, p21, p27 and promotes apoptosis by decreasing the levels of gene products linked to pro-survival mechanisms [10].

However, the clinical efficacy of curcumin is to a small extent influenced by its water solubility, bioavailability, instability and rapid metabolism and excretion [11,12]. Curcumin's low bioavailability is due to its chemical and biological instability under physiological conditions [13]. One of the promising strategies for handling the shortcomings of curcumin that several researchers have reported is combining modernized advanced drug delivery systems with new synthetic curcumin analogues, nanoparticles, and metal complexes. The modified curcumin has been shown to overcome the demerits of curcumin while improving solubility, bioavailability, and therapeutic efficacy; hence, more bioactivity is observed with less toxicity. These changes are possible in any of the active sites such as aromatic side chain, linker chain, diketo functionality and active methylene group [14–16].

It was found from SAR studies that the stability and pharmacological activity as well as solubility would be increased on converting the diketone form of curcumin into a monoketone form. This modification has attracted much attention because the 1,3-dicarbonyl system is highly reactive and catalyzes degradation by hydrolysis [11]. In this context, Marchiani and Xu et al., have reported that their compounds showed enhanced anticancer activity and remained stable after 72 hours when featuring a cyclopentanone ring and additionally the metabolism for the diaryl pentadienone was significantly decreased both in rate and extent as compared to curcumin [17,18].

In addition to changing the diketone version of curcumin into the monoketone variant, it has been noted that replacing the benzene ring with a heteroaromatic ring might preserve or even improve the cytotoxic properties of curcumin's monoketone derivatives [19]. Heterocyclic compounds that contain nitrogen are particularly noteworthy and unique in the fields of synthetic and medicinal chemistry. Among these, pyrazoles, which are five-membered heteroaromatic rings, represent a highly significant category of compounds that play a crucial role as key bioactive intermediates in the quest for new therapeutic agents in medicinal research [20,21]. Pyrazole-based structures that hold pharmacological importance exhibit a diverse range of activities, including antiviral, antibacterial, antimalarial, anti-inflammatory, antidiabetic, antiglaucoma, and most significantly, anticancer effects [22–27].

Based on these observations in literature, 15 curcuminoids were synthesized and characterized by the incorporation of the cyclopentanone, cyclohexanone, and cycloheptanone moiety in the five-carbon linker of curcumin and by the replacement of the aromatic benzene ring with the nitrogen-containing heterocyclic moiety pyrazole. All curcuminoids were screened for in vitro cytotoxicity,

 doi:10.20944/preprints202501.1735.v1

and the most active curcuminoid 5i was further studied experimentally through in vitro and in vivo approaches to unveil the molecular mechanisms underlying its cytotoxic activity [Figure 1].

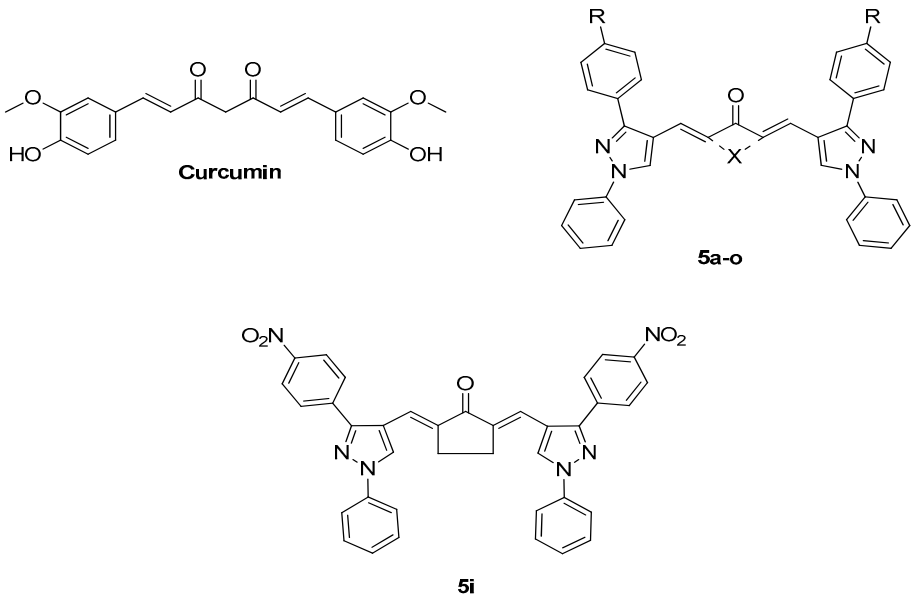

Figure 1. Structures of curcumin and our synthesized curcuminoids, Curcuminoid 5i which was studied extensively.

2. Results

2.1. Chemistry

Synthesis and Characterization of Curcuminoids

A set of fifteen curcuminoids, 5a-o, were synthesized according to Scheme 1, Figure 2. The reaction between phenyl hydrazine (**1**) in a 0.05 molar solution with substituted acetophenone (**2**) in 30 mL of ethanol at reflux for 4 h, resulted in the formation of 1-phenyl-2-(1-(4-substituted)ethylidene)hydrazine, **3**. The Vilsmeier-Haack reagent was used to obtain the aldehyde derivative **4** of3-(4-substituted)-1-phenyl-1H-pyrazole-4-carbaldehyde in satisfactory yield from refluxing it with phosphorus oxychloride and DMF at low temperature between 0-5°C. Lastly, the reactions between ketones (0.001 M) and methanolic KOH (0.008 M) with the THF solutions of 3-(4-substituted)-1-phenyl-1H-pyrazol-4-carbaldehyde (**4**) (0.002 M) gave good yields of bis((3-(4-substituted)-1-phenyl -1H-pyrazol -4 -yl)methylene)ketone analogs (**5a-o**).

 doi:10.20944/preprints202501.1735.v1

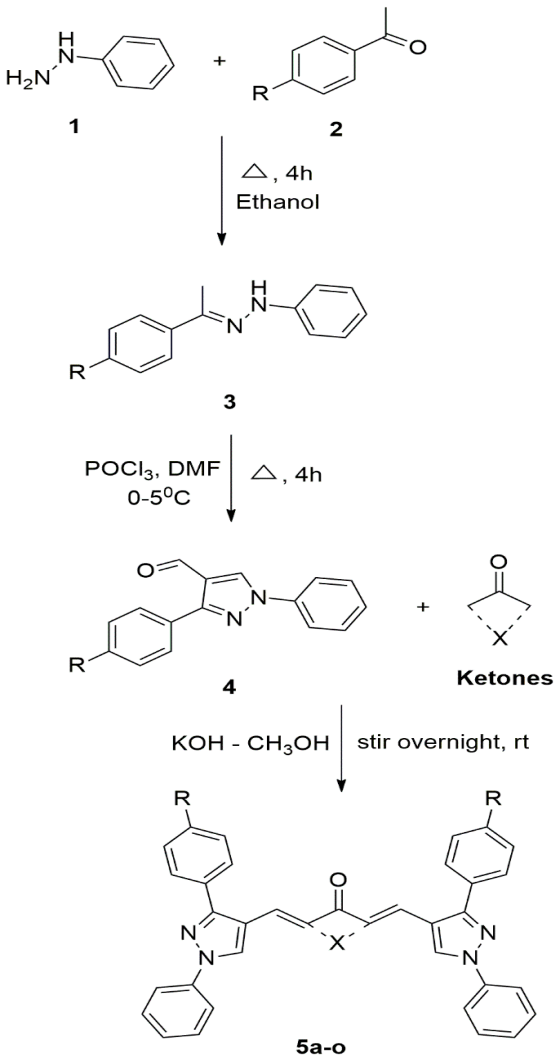

Compound	R	X
5a	H	-$(CH_2)_3$-
5b	OCH_3	-$(CH_2)_3$-
5c	CH_3	-$(CH_2)_3$-
5d	NO_2	-$(CH_2)_3$-
5e	Cl	-$(CH_2)_3$-
5f	H	-$(CH_2)_2$-
5g	OCH_3	-$(CH_2)_2$-
5h	CH_3	-$(CH_2)_2$-
5i	NO_2	-$(CH_2)_2$-
5j	Cl	-$(CH_2)_2$-
5k	H	-$(CH_2)_4$-
5l	OCH_3	-$(CH_2)_4$-
5m	CH_3	-$(CH_2)_4$-
5n	NO_2	-$(CH_2)_4$-
5o	Cl	-$(CH_2)_4$-

Figure 2. Synthesis of curcuminoids 5a-o.

 doi:10.20944/preprints202501.1735.v1

All the synthesized curcuminoids (5a-o) were characterized by the spectroscopic data of FTIR, $^{1}H/^{13}C$ NMR, and HR-MS. Stretching absorption bands for C-H aromatic were observed in the range 3082-3009 cm^{-1}, C-H aliphatic in 2962–2911 cm^{-1}, C=O in 1750-1685 cm^{-1} and C=C aromatic in 1611–1524 cm^{-1} for compounds 5a-o. Curcuminoid 5i exhibited characteristic vibration at 1685 cm^{-1} for C=O.

The ^{1}H NMR spectra of 5a-o showed significant signals for pyrazole protons between δ 8.81-7.73 ppm and for aromatic protons between δ 7.98-6.98 ppm. The cyclic ketones with different chain lengths showed the presence of -CH_2- groups between δ 4.2-1.75 ppm. The range for methyl protons in curcuminoids 5c, 5h, and 5m was found to be between δ 2.51-2.35 ppm while that for methoxy protons in curcuminoids 5b, 5g, and 5l was found to be between δ 3.86-3.85 ppm. For curcuminoid 5i, prominent signals were observed at δ 3 .00 ppm for -CH_2- groups, at δ 8 .18 ppm for pyrazole protons, and between δ 7.80-7.35 ppm for aromatic protons.

The ^{13}C NMR spectra of 5a-o, exhibited peaks in the range of δ 207-162 ppm for C=O of ketones, peaks in the range of δ 160-114 ppm for aromatic carbons, peaks in the range of δ 55.45-55.42 ppm for methoxy carbons and at δ 21.59-21.45 ppm for methyl carbons on benzene ring. Methylene carbon peaks of -$(CH_2)_2$, -$(CH_2)_3$ and-$(CH_2)_4$ of ketones was shown between δ 29.42-21.47 ppm. For curcuminoid 5i, prominent signals were noted at δ 207.17 ppm for C=O and between δ 153.90-118.14 ppm for aromatic carbons and at δ 26.57 ppm for methylene carbons in the cyclic ketone -$(CH_2)_2$.

The HR-MS spectrum of curcuminoids 5a-o showed molecular ion peak corresponding to their molecular weights; hence, the identity of all the compounds is confirmed. For curcuminoid 5i, the mass was corroborated by HRMS with the molecular peak exhibited at 635.2040 (calc. 634.6395).

2.2. In Vitro Studies

2.2.1. In Vitro Cytotoxicity Evaluation

All curcuminoids (5a-o) were initially screened at a wide range of concentrations, including 0.1, 1, 10, and 100 μM, with curcumin serving as the positive control (Table 1). Based on the MTT assay conducted on MOLT-4 cells, it can be inferred that most of the individual compounds exhibited excellent cytotoxic activity; only compounds 5b, 5c, and 5e showed very weak activity compared to that of curcumin. From those first-screened compounds four were selected to be tested at narrow range concentrations of 20, 40, 60, 80, 100, 200, and 400 nM. The most potent was compound 5i which was further analyzed to reveal the mechanism of action.

Table 1. *In vitro* cytotoxicity data of synthesized compounds (5a-o) on MOLT-4 cell line.

Compound	IC_{50} (μM)
5a	34.36 ± 3.24
5b	134.59 ± 1.55
5c	8336811.85 ± 494.90
5d	36.39 ± 1.78
5e	207969.67 ± 86.00
5f	0.92 ± 0.00
5g	12.44 ± 0.44
5h	49.98 ± 10.77
5i	0.10 ± 0.01
5j	11.91 ± 1.48
5k	0.58 ± 0.00
5l	16.15 ± 0.31
5m	46.24 ± 4.18
5n	8.97 ± 2.62
5o	9.23 ± 0.04
Curcumin	61.66 ± 2.26

Tables may have a footer.

 doi:10.20944/preprints202501.1735.v1

2.2.2. In Vitro Cytotoxicity Evaluation in Cell Lines

Based on the broad range data obtained from section 2.2.1, the cytotoxic activity of curcuminoid 5i at a narrow range of 20-200 nM was determined by precursor DMSO vehicle-controlled treatment followed by addition to MOLT-4 and HEK293 cells for 48 h, followed by addition of MTT and resazurin. MTT is a yellow, water-soluble tetrazolium dye that is mainly reduced by mitochondrial dehydrogenases in cells, leading to the formation of purple formazan granules. On the other hand, resazurin is a viability dye working on the principle that in living cells it gets reduced by the respiratory chain in mitochondria to form the non-fluorescent blue resazurin which produces red fluorescent dye (resorufin). There are more than two examples here showing at least some reduction in cell number due to treatment with 5i at higher concentrations. The activity of 5i was primarily screened using MTT and resazurin in MOLT-4 cells at higher concentrations, showing reduction in cell number. Both assays gave an IC_{50} within the range of 100 nM-200 nM. (Figure 3a, 3b).

In order to have a more precise idea of the compound's potential in non-tumorigenic context, an investigation was conducted to evaluate the efficiency of this compound in HEK293 cell line, which are progenitor human embryonic kidney cells. As displayed in Figure 3c, the IC_{50} value obtained in HEK293 falls between 10-50 μM which is higher than reported in leukemia cells at the above said concentration range. These observations along with the fact that curcuminoid 5i shows efficacy on leukemia cells with no effect on other (previously described) non-cancer cells populations draw attention to its potential as a target for leukemia therapy with broader application.

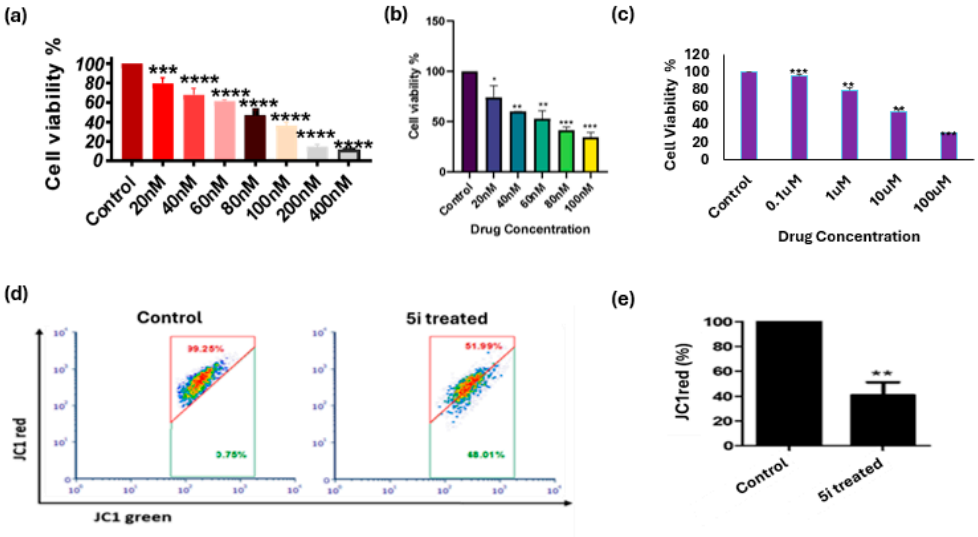

Figure 3. *In vitro* evaluation of 5i on cellular processes: (a) Cytotoxicity evaluation of 5i in MOLT-4 cell line using MTT assay (b) Cytotoxicity evaluation of 5i in MOLT-4 cell line using resazurin assay (c) Cell viability in HEK293 cells upon the treatment of 5i (d) JC-1 staining indicating change in mitochondrial membrane potential (MMP) upon 5i treatment (e) Quantification of MMP is depicted as a bar graph after 48 h treatment of 5i on MOLT-4 cells. Every experiment was repeated three times and represented as histograms. The p-value was calculated between the control and 5i treated groups (** $p < 0.005$).

2.2.3. **5i** Alters Mitochondrial Membrane Potential (MMP) (Δψm)

The effect of **5i** on the cytotoxicity mechanism was revealed by exposing the MOLT-4 cell line to **5i** for 48 h and then staining with JC-1. In viable cells, JC-1, a cationic dye, accumulates in the mitochondria forming aggregates that result in red fluorescence. In apoptotic cells, the mitochondrial membrane is leaky to JC-1 and hence no aggregates are formed resulting in green fluorescence. Figure 3d, 3e shows flow cytometry analysis where there is an increase in the green population upon treatment with **5i** indicating damage to mitochondria. There was no evidence of mitochondrial damage in the vehicle control.

 doi:10.20944/preprints202501.1735.v1

2.2.4. 5i Treatment-Induced Apoptotic Activation in MOLT-4 Cells

Changes in mitochondrial proteins were evaluated tounravel molecular mechanism of 5i induced change in MMP. Western blotting was performed to evaluate the protein expression levels before and after treatment (Figure 4a).Western blot analysis showedsignificantly increased levels of BAK, the pro-apoptotic protein located in the outer mitochondrial membrane.The levels of BCL-2, the anti-apoptotic protein, did not show a significant reduction (Figure 4b), the ratio of the BAK: BCL2 was altered explaining the observed change in MMP. A change in MMP was further confirmed by assaying the levels of Cytochrome C, which escapes from mitochondria due to altered MMP. An increase in cytochrome C although nonsignificant was observed in MOLT-4 cells. Downstream of the release of Cytochrome C is the formation of apoptosome complex with Apaf-1 and Caspase 9 leading to activation of Caspase 9, which activates Caspase 3. The treatment with 5i markedly enhanced the levels of the cleaved caspase-3 indicating activation of Caspase 3 (Figure 4a, 4b).

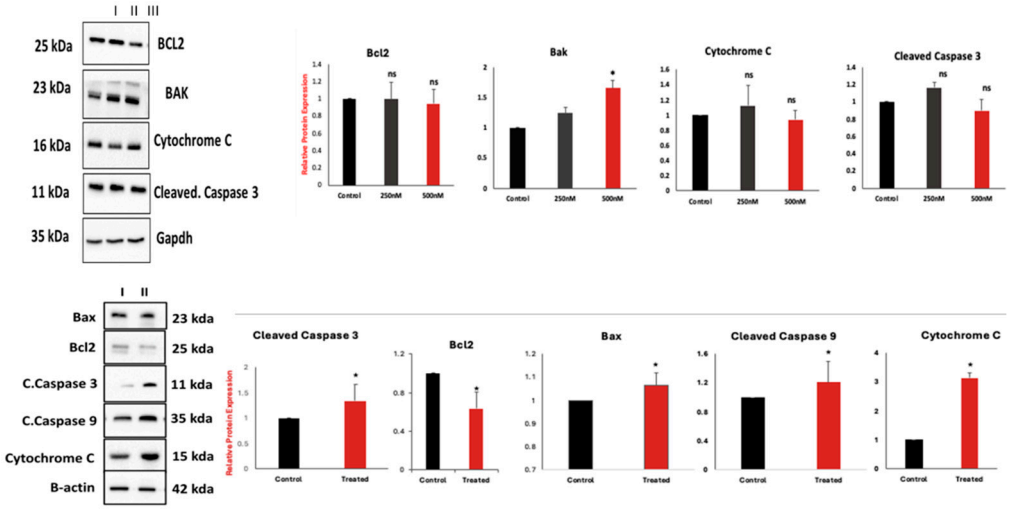

Figure 4. *In vitro* and *In vivo* Western Blot Analysis of **5i** Treatment a) Western blot images of apoptotic protein markers in MOLT-4 cellsb) Quantification of apoptotic protein markersc) Western blot images of apoptotic protein markers in DLA control and treated tumor d)Quantification of apoptotic protein markers.A one-sample t-test was performed, and p-values were calculated to compare the control and **5i**treated groups.

Caspases, as a general class, are cysteine-dependent aspartate proteases that are critically involved in the execution phase of apoptosis; their activation indicates an adherence to the intrinsic/ mitochondrial-mediated cell death process. Although there were signs of induction of intrinsic pathway of apoptosis in MOLT-4 cells, it was not very convincing. The observed cell death in MOLT-4 cells might be driven by other mechanisms not assayed here.

Having tested the drug in an *in vitro* cell model and deciphered the molecular mechanism of cell death as mitochondria-mediated, we wanted to test the impact of drug *in vivo*. Since we do not have syngeneic mouse models of leukemia, we decided to test the drug on mouse lymphoma model. We observed a reduction in tumors in the mouse model described below. We extracted protein from tumor of control and treated animals and performed western blot analysis to check whether 5i induced intrinsic pathway of apoptosis. Interestingly, we obtained significant change in the mitochondrial membrane protein Bcl-2 and Bax (Figure 4c, 4d) and markers of the apoptotic pathway cleaved caspase 9, cleaved caspase 3 and cytochrome C in DLA tumors, indicating differences in activity of the drug in two different conditions. Further experiments on metabolism of the drug in MOLT-4 and DLA model might explain the observed differences.

2.3. In Vivo Studies

5i Induced Tumor Regression in DLA Mouse Model Without Observable Toxicity

 doi:10.20944/preprints202501.1735.v1

To generate the mouse model, DLA cells were injected in the left thigh region of Swiss albino mice to induce the tumor.After inducing the tumor, the mice were segregated into 5 controls and 5 treatments.The treatment group was administered intraperitoneally, daily, 50 mg/kg body weight of **5i** for 31 days, thus making it 30 doses.

Throughout the treatment period, tumor volume was measured to check the effect of 5i on tumor reduction. Figure 5a shows an increase in tumor volume over 30-day period in control mouse. In contrast, the tumor volume did not increase in the presence of 5i, indicating that 5i did not allow tumor growth. As mentioned in the previous section, this no growth in tumour can be explained by induction of mitochondria mediated cell death in DLA cells.

To observe if there were any visible signs of drug toxicity, the body weight was recorded along the time frame of the experiment. No significant reduction in body weight was observed in treatment groups (Figure 5b). Further, to check whether drug affected liver or kidney as these are sites of drug metabolism and excretion, the liver, kidney and spleen apart from tumour was collected and their morphology assessed. As is apparent from Figure 5c, there was marked tumor reduction. In contrast, no apparent change between control and 5i treated liver and kidney indicated no apparent toxicity. The decrease in spleen size was observed concomitant with decrease in tumour volume indicating clearance of tumour cells by the spleen. This is not observed in control tumor where the tumor burden is high. The spleen enlarged to perform its function. One way to measure tumor reduction is also to observe spleen size.

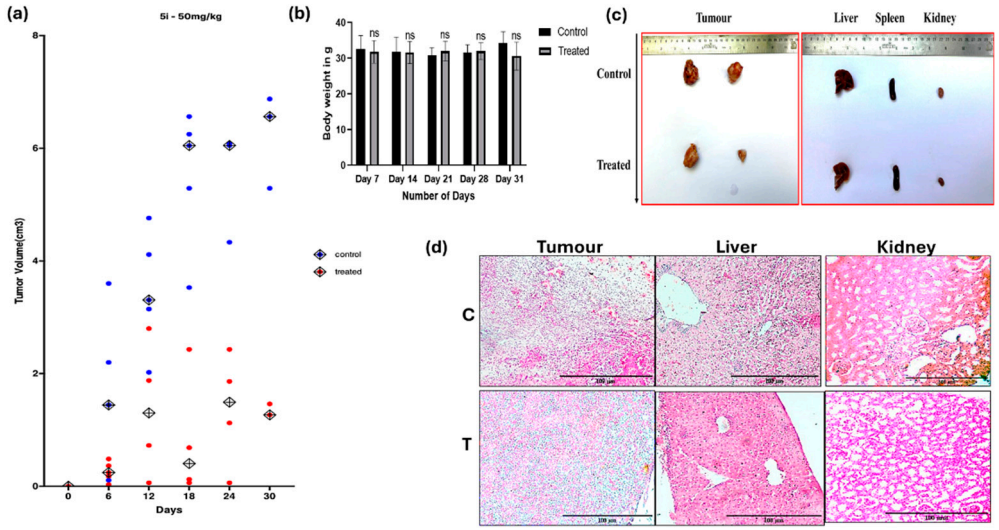

Figure 5. Histological and Morphological analysis of control (C) and **5i** treated (T) DLA mouse model: a) Tumor volume decreased significantly after 30 days of treatment with **5i** b) Body weight measurement of control and treated animal c) Reduction in tumour size and no observable difference in liver, spleen and kidney morphology was observed d) No difference in the cellular organization of liver and kidney was observed in control vs treated animal.

Since no morphological change was observed, to detect any cellular changes in the tissues we made sections of the tissues. As is apparent in Figure 5d, the organization of the liver and kidney was intact in both control and drug treated sample. The tissue architecture was close to normal in **5i** treated animals confirming no apparent toxicity. Further experiments using the liver and kidney function tests will validate the observations made for the curcuminoid **5i**.

3. Discussion

The two main challenges of cancer treatment are metastasis and recurrence of the disease [28]. Despite all these, it remains a challenge to develop an anticancer drug with low drug toxicity. Recent studies have shown that survival rates in leukemia and lymphoma are lower compared to other

 doi:10.20944/preprints202501.1735.v1

cancer types with weak drug responses in patients that have had extensive targeted therapy [29]. Curcumin is associated with antioxidant, antiinflammatory, antimicrobial, anticancer, and antimutagenic properties; thus, it can be used as a dietary supplement for various health conditions [8]. Curcumin acts at initiation, promotion, and progression stages of cancer through its action on diverse genes and proteins. The antioxidant activity as well as ROS scavenging activity of curcumin is correlated with its anticancer activity because reactive oxygen species affect several kinds of cancers. These include leukemia, lymphoma, melanoma and sarcoma genitourinary, breast, ovarian, head and neck, lung, and neurological cancers [30].

Several signaling pathways identified in the anticancer effects of curcumin overlap with inhibition of the NF-κB transcription factor activation. Given that NF-κB-regulated gene products include apoptosis inhibitors (Bcl-2, Bcl-XL, TRAF), regulators of the cell cycle (cyclin D), growth factors (interleukins, VEGF), growth factor receptors, and matrix metalloproteinases, inhibition of NF-κB trans-activating activity would result in down regulation of its targets that govern numerous processes involved in cell proliferation [31].

The activity of curcumin is restricted due to its poor solubility in water and low bioavailability. Several strategies are under research to tackle these problems, such as the following: new natural analogs of curcumin originating from turmeric; natural curcumin analogs from other plant species; production of synthetic curcumin analogs through the change of functional groups; reformulation of curcurmin with different oils; encapsulation of curcurmin in various amphiphilic copolymers [32] and structural modification or synthesis of analogs. These modified structures show increased biological activity over standard curcumin, indicating a promising profile for antitumor activity through apoptosis induction alongside inhibition of various cell line growth and proliferation [11,32].

The current set of curcuminoids were designed by incorporating cyclic ketones in the five-carbon linker analogue of curcumin and by incorporating 3-(4-substituted)-1-phenyl-1H-pyrazole-4-carbaldehyde in place of the aromatic benzene ring. This strategy was employed as derivatives of curcumin with the cyclic ketone group were found to inhibit the growth of tumor by inhibiting the cell cycle progression [33], induce apoptosis [34], trigger cell cycle arrest in the G2/M phase [35], exhibit stronger antitumor activities than curcumin by activating ROS-YAP-JNK signaling pathway by inducing mitochondrial dysfunction and apoptosis [36] and inhibit cell growth involving multiple molecular targets, including ROS and ER stress [37]. Further, analogs of curcumin having a cyclopentanone ring were found to possess cytotoxicity with IC50 values below 1 μM and 1.35 μM against MOLT-4, HeLa, PC3, DU145, KB cancer cell lines [38] and leukemia K-562 cell lines respectively. Some even showed effectiveness against leukemia RPMI-8226 and renal RXF-393 cell lines with GI50 values of 0.6 and 0.5 μM, respectively [39].

The current study elucidates the mechanism of cell death by which curcuminoid 5i induces potent antitumorigenic activity in vitro against the leukemic cancer cell line and mouse lymphoma model. A drug can cause cell death through several mechanisms, as already pointed out [40]. In particular, curcumin derivatives are known to bring about apoptosis by disturbing mitochondrial membrane potential and also by initiating a cascade of caspase pathways [41,42]. The effect of 5i was similar but achieved at a nanomolar concentration causing apoptotic cell death intrinsically on MOLT-4 cancer cell lines. These were evidenced by the subsequent change in mitochondrial membrane potential and upregulation of pro-apoptotic proteins such as Bax and cytochrome-c while downregulating anti-apoptotic protein Bcl2. Post this, it was observed that 5i induced changes in Bcl2-Bax ratios in MOLT-4 cells post-treatment which correlated well with the theory that Bax oligomerizes with Bak, forms pores on the mitochondrial membrane leading to the release of proteins like cytosolic cytochrome C [43].

Due to the encouraging in vitro results, the in vivo activity of 5i was tested in the DLA model. Significant regression of tumor growth compared to control groups was observed with 5i at 50 mg/kg dose with at least 30 doses in treated groups of DLA model. Besides this, organ damage was very mild due to the potency of 5i. Moreover, preliminary studies on LFT and KFT, showed no change in

 doi:10.20944/preprints202501.1735.v1

urea, BUN and ALT levels showing that 5i had very low organ toxicity (data not shown). The studies are ongoing to evaluate the pharmacokinetics and pharmacodynamics of the drug.

H&E staining in the samples of control tissue showed more packed and stained nuclei than in the samples of treated tissue. This indicates that 5i was primarily directed against proliferating cells. The markers for the intrinsic apoptotic pathway, Bax, cleaved caspase3, and cleaved caspase 9, were significantly increased in the tumor samples from treated mice compared to those from untreated controls. These results thus demonstrate that 5i at lower doses inhibits growth on DLA tumor mouse models and induces cytotoxicity through the intrinsic pathway of apoptosis with minimal side effects.

4. Materials and Methods

4.1. Chemistry

Synthesis and Characterization of Curcuminoids

Solvents and reagents were pretested for purity. Silica gel 60 GF_{254} plates from Merck were used to monitor the reaction progress by TLC. The melting point was measured using a DBK melting point apparatus. FTIR spectra were obtained using IR-grade KBr, and the diffuse reflectance technique was employed on the Jasco FTIR 460+. NMR $^{1}H/^{13}C$ spectra were recorded between 400 and 500/100 MHz in DMSO-d_6 and $CDCl_3$ on Bruker (Ultraspec AMX 400) and JEOL RESONANCE (JNM-ECZ400S). All values of chemical shift (δ) are in ppm with TMS as reference. The HR-MS spectra were obtained from the Institution of Excellence, Vijnana Bhavan, Mysuru, on the Waters, USA (Xevo G2-XS QTof). Compounds 1-phenyl-2-(1-(4-substituted)ethylidene)hydrazine and 3-(4-substituted)-1-phenyl-1H-pyrazole-4-carbaldehyde were synthesized as described in the literature. [44,45].

General procedure for the synthesis of 2,6-bis((3-(4-substituted)-1-phenyl-1*H*-pyrazol-4-yl)methylene)ketone (5a-o)

KOH (0.008 M) in methanol was prepared, then the batch of tetrahydrofuran with 3-(4-substituted)-1-phenyl-1H-pyrazole-4-carbaldehyde (0.002 M) was added. The mixture was stirred for 20 mins under ice-cold conditions. Ketone (0.001 M) was added dropwise. Then the resulting mixture was stirred at room temperature overnight and then poured into ice-cold water (100 mL). The mixture was neutralized with dilute hydrochloric acid to give a solid that was recrystallized from chloroform-methanol.

(2*E*,6*E*)-2,6-bis((1,3-diphenyl-1*H*-pyrazol-4-yl)methylene)cyclohexan-1-one (5a)

Yield 78%, m.p.260-262°C; IR (KBr) νmax/cm^{-1}: 3057, 2939, 1659, 1600, 1503, 1275, 1168, 1059; δ/ppm for ^{1}H NMR (400 MHz, DMSO-d_6): 1.86 (s, 2H, alkyl -CH_2-), 2.93 (s, 4H, alkyl (-CH_2-)$_2$), 7.36 (t, 2H, Ar, *J*=16), 7.46-7.61 (m, 16H, Ar), 8.00 (d, 6H, Ar, *J*=8), 8.82 (s, 2H, Ar); ^{13}C NMR (100 MHz, $CDCl_3$, δ/ppm): 188.23, 154.85, 139.64, 134.30, 132.37, 129.62, 128.96, 128.81, 128.60, 127.73, 127.53, 127.12, 119.41, 117.42, 28.92, 22.46; HR-MS m/z: [$C_{38}H_{30}N_4O$]$^+$, 559.2488 (calc. 558.6710).

(2*E*,6*E*)-2,6-bis((3-(4-methoxyphenyl)-1-phenyl-1*H*-pyrazol-4-yl)methylene) cyclohexan-1-one (5b)Yield 81%; m.p.212-216°C; IR (KBr) νmax/cm^{-1}: 3049, 2962, 1654, 1596, 1504, 1252, 1177, 1058; ^{1}H NMR (400 MHz, $CDCl_3$, δ/ppm): 1.96 (p, 2H, alkyl -CH_2-, J=28), 2.88 (t, 4H, alkyl (-CH_2-)$_2$, J=12), 3.85 (s, 6H, -CH_3-), 7.00 (d, 4H, Ar, *J*=4), 7.32 (t, 2H, Ar, *J*=16), 7.48 (t, 4H, Ar, *J*=16), 7.65 (d, 4H, Ar, *J*=12), 7.79 (d, 4H, Ar, *J*=12), 7.84 (s, 2H, Ar), 8.12 (s, 2H, Ar); ^{13}C NMR (100 MHz, $CDCl_3$, δ/ppm): 188.28, 159.98, 154.74, 139.72, 134.08, 130.21, 129.61, 127.90, 127.38, 127.00, 124.92, 119.39, 117.28, 114.27, 55.45, 28.91, 22.45; HR-MS *m*/*z*: [$C_{40}H_{34}N_4O_3$]$^+$, 619.2710 (calc. 618.7230).

(2*E*,6*E*)-2,6-bis((1-phenyl-3-(p-tolyl)-1*H*-pyrazol-4-yl)methylene)cyclohexan-1-one (5c) Yield 80%; m.p.240-246°C; IR (KBr) νmax/cm^{-1}: 3018, 2925, 1659, 1598, 1503, 1227, 1172, 1060; ^{1}H NMR (400 MHz, DMSO- d_6, δ/ppm): 1.87 (s, 2H, alkyl -CH_2-), 2.36 (s, 6H, -CH_3-), 2.93 (s, 4H, alkyl (-CH_2-)$_2$), 7.31-7.37 (m, 6H, Ar), 7.47-7.54 (m, 10H, Ar), 7.99 (d, 4H, Ar, *J*=8), 8.80 (s, 2H, Ar); ^{13}C NMR (100 MHz, $CDCl_3$, δ/ppm): 188.19, 154.95, 139.68, 138.43, 134.14, 129.58, 129.50, 128.84, 127.83, 127.42, 127.00, 119.37, 117.38, 28.91, 22.46, 21.48; HR-MS *m*/*z*: [$C_{40}H_{34}N_4O$]$^+$, 587.2831 (calc. 586.7242).

 doi:10.20944/preprints202501.1735.v1

(2*E*,6*E*)-2,6-bis((3-(4-nitrophenyl)-1-phenyl-1*H*-pyrazol-4-yl)methylene)cyclohexan-1-one (5d) Yield 40%; m.p.>290°C; IR (KBr) νmax/cm^{-1}: 3069, 2953, 1662, 1597, 1537, 1341, 1269, 1162, 1067; ^{1}H NMR (400 MHz, $CDCl_3$, δ/ppm):8.35-8.33 (d, 4H, Ar, *J*=8 Hz), 8.17 (s, 2H, Ar), 7.94-7.92 (d, 4H,Ar, *J*= 8 Hz), 7.83-7.79 (t, 6H, triplet, Ar, *J*=24 Hz), 7.55-7.51 (t, 4 H, Ar, *J*=16 Hz), 7.41-7.37 (t, 2H, Ar, *J*=16 Hz), 7.25 ($CDCl_3$), 2.9-2.88 (t, 4H, alkyl (-CH_2-)$_2$, *J*= 8 Hz), 1.980 (p, 2H, alkyl -CH_2-); ^{13}C NMR (100 MHz, $CDCl_3$, δ/ppm): 152.14, 147.71, 139.45, 137.29, 136.99, 136.35, 135.18, 129.80, 129.45, 128.02, 127.76, 126.86, 124.10, 119.65, 117.80, 31.06, 28.79; HR-MS *m*/*z*: [$C_{38}H_{28}N_6O_5$]$^+$, 649.2195 (calc. 648.6661).

(2*E*,6*E*)-2,6-bis((3-(4-chlorophenyl)-1-phenyl-1*H*-pyrazol-4-yl)methylene) cyclohexan-1-one (5e) Yield 75%; m.p.130-136°C; IR (KBr) νmax/cm^{-1}: 3055, 2951, 1660, 1596, 1223, 1162, 1060; ^{1}H NMR (400 MHz, DMSO- d_6, δ/ppm): 1.85 (p, 2H, alkyl -CH_2-), 2.92 (t, 4H, alkyl (-CH_2-)$_2$), 7.37 (t, 2H, Ar, *J*=12), 7.51-7.63 (m, 14H, Ar), 8.00 (d, 4H, Ar, *J*=8), 8.83 (s, 2H, Ar); ^{13}C NMR (100 MHz, $CDCl_3$, δ/ppm): 188.14, 153.65, 139.55, 134.70, 134.47, 130.87, 130.15, 129.68, 129.04, 127.60, 127.38, 127.32, 119.48, 117.38, 28.85, 22.38; HR-MS *m*/*z*: [$C_{38}H_{28}Cl_2N_4O$]$^+$, 627.1785 (calc. 627.5611).

(2*E*,5*E*)-2,5-bis((1,3-diphenyl-1*H*-pyrazol-4-yl)methylene)cyclopentan-1-one (5f) Yield 84%; m.p.250-252°C; IR (KBr) νmax/cm^{-1}: 3056, 2913, 1680, 1600, 1504, 1224, 1171, 1065; ^{1}H NMR (400 MHz, DMSO- d_6, δ/ppm): 3.09 (s, 4H, alkyl (-CH_2-)$_2$), 7.32-7.39 (m, 4H, Ar), 7.47-7.61 (m, 14H, Ar), 8.00 (s, 4H, Ar), 8.85 (s, 2H, Ar); ^{13}C NMR (100 MHz, $CDCl_3$, δ/ppm): 194.58, 155.12, 139.61, 136.56, 132.17, 129.67, 129.51, 129.08, 128.87, 128.75, 127.67, 127.56, 127.32, 123.94, 119.59, 119.32, 118.19, 26.58; HR-MS *m*/*z*: [$C_{37}H_{28}N_4O$]$^+$, 545.2332 (calc. 544.6444).

(2*E*,5*E*)-2,5-bis((3-(4-methoxyphenyl)-1-phenyl-1*H*-pyrazol-4-yl)methylene)cyclopentan-1-one (5g) Yield 86%; m.p.220-224°C; IR (KBr) νmax/cm^{-1}: 3051, 2912, 1679, 1611, 1530, 1498, 1253, 1174, 1066; ^{1}H NMR (400 MHz, $CDCl_3$, δ/ppm): 3.01 (s, 4H, alkyl (-CH_2-)$_2$), 3.86 (s, 6H, -CH_3-), 7.01 (d, 4H, Ar, *J*=4), 7.34 (t, 2H, Ar, *J*=12), 7.50 (t, 4H, Ar, *J*=16), 7.62-7.65 (m, 6H, Ar), 7.81 (d, 4H, Ar, *J*=4), 8.17 (s, 2H, Ar); ^{13}C NMR (100 MHz, $CDCl_3$, δ/ppm): 194.55, 160.05, 154.84, 139.59, 136.39, 130.29, 129.62, 127.44, 127.15, 124.64, 123.97, 119.47, 117.96, 114.29, 55.43, 26.50; HR-MS *m*/*z*: [$C_{39}H_{32}N_4O_3$]$^+$, 605.2559 (calc. 604.6964).

(2*E*,5*E*)-2,5-bis((1-phenyl-3-(p-tolyl)-1*H*-pyrazol-4-yl)methylene)cyclopentan-1-one (5h) Yield 85%; m.p.234-238°C; IR (KBr) νmax/cm^{-1}: 3062, 2915, 1655, 1584, 1503, 1224, 1173, 1015; ^{1}H NMR (400 MHz, $CDCl_3$, δ/ppm): 2.41 (s, 6H, - CH_3-), 3.01 (s, 4H, alkyl (-CH_2-)$_2$), 7.29 (d, 2H, Ar, *J*=8), 7.35 (t, 2H, Ar, *J*=12), 7.50 (t, 4H, Ar, *J*=12), 7.59 (d, 4H, Ar, *J*=4), 7.66 (s, 2H, Ar), 7.81 (d, 4H, Ar, *J*=12), 8.18 (s, 2H, Ar); ^{13}C NMR (100 MHz, $CDCl_3$, δ/ppm): 194.71, 155.40, 139.92, 138.79, 136.63, 129.81, 129.71, 129.51, 129.12, 127.61, 127.38, 124.24, 119.76, 118.40, 26.79, 21.60; HR-MS *m*/*z*: [$C_{39}H_{32}N_4O$]$^+$, 573.2653 (calc. 572.6976).

(2*E*,5*E*)-2,5-bis((3-(4-nitrophenyl)-1-phenyl-1*H*-pyrazol-4-yl)methylene)cyclopentan-1-one (5i) Yield 65%; m.p.>290°C; IR (KBr) νmax/cm^{-1}: 3070, 2933, 1685, 1572, 1534, 1338, 1226, 1168,1090; ^{1}H NMR (400 MHz, $CDCl_3$, δ/ppm): 3.01 (s, 4H, alkyl (-CH_2-)$_2$), 7.37 (t, 2H, Ar, *J*=16), 7.44-7.53 (m, 8H, Ar), 7.60-7.64 (m, 6H, Ar), 7.80 (d, 4H, *J*=8), 8.18 (s, 2H); ^{13}C NMR (100 MHz, $CDCl_3$, δ/ppm): 207.17, 194.45, 153.91, 139.54, 136.77, 130.28, 129.73, 129.12, 127.67, 127.51, 123.57, 119.64, 118.14, 31.06, 26.57; HR-MS *m*/*z*: [$C_{37}H_{26}Cl_2N_4O$]$^+$, 635.2040 (calc. 634.6395).

(2*E*,5*E*)-2,5-bis((3-(4-chlorophenyl)-1-phenyl-1*H*-pyrazol-4-yl)methylene) cyclopentan-1-one (5j) Yield 83%; m.p.204-208°C; IR (KBr) νmax/cm^{-1}: 3050, 2911, 1680, 1595, 1500, 1230, 1171, 1065; ^{1}H NMR (400 MHz, DMSO- d_6, δ/ppm): 3.08 (s, 4H, alkyl (-CH_2-)$_2$), 7.28 (s, 2H, Ar), 7.40 (t, 4H, Ar, *J*=8), 7.57 (t, 4H, Ar, *J*=20), 7.62-7.65 (m, 8H, Ar, *J*=12), 8.00-8.02 (d, 4H, Ar, *J*=8), 8.86 (s, 2H, Ar); ^{13}C NMR (100 MHz, $CDCl_3$, δ/ppm): 188.13, 153.92, 139.53, 138.71, 136.76, 130.29, 129.74, 129.13, 127.84, 127.68, 127.52, 125.24, 123.58, 119.64, 118.14, 26.57; HR-MS *m*/*z*: [$C_{37}H_{26}Cl_2N_4O$]$^+$, 613.1554 (calc. 613.5345).

(2*E*,7*E*)-2,7-bis((1,3-diphenyl-1*H*-pyrazol-4-yl)methylene)cycloheptan-1-one (5k) Yield 65%; m.p.210-215°C; IR (KBr) νmax/cm^{-1}: 3052, 2919, 1662, 1597, 1230, 1145, 1061; ^{1}H NMR (400 MHz, $CDCl_3$, δ/ppm): 1.98 (s, 4H, alkyl (-CH_2-)$_4$), 2.75 (s, 4H, alkyl (-CH_2-)$_4$), 7.33 (t, 2H, Ar, *J*=12), 7.39-7.51 (m, 12H, Ar) 7.72 (d, 4H, Ar, *J*=8), 7.80 (d, 4H, Ar, *J*=8), 8.14 (s, 2H, Ar); ^{13}C NMR (100 MHz, $CDCl_3$, δ/ppm): 197.58, 154.54, 139.77, 139.63, 132.46, 129.65, 128.93, 128.81, 128.64, 128.56, 127.08, 126.57, 126.50, 119.47, 117.01, 28.46, 26.66; HR-MS *m*/*z*: [$C_{39}H_{32}N_4O$]$^+$, 573.2656 (calc. 572.6976).

 doi:10.20944/preprints202501.1735.v1

(2*E*,7*E*)-2,7-bis((3-(4-methoxyphenyl)-1-phenyl-1*H*-pyrazol-4-yl)methylene) cycloheptan-1-one (5l) Yield 57%; m.p.115-120°C; IR (KBr) νmax/cm^{-1}: 3070, 2912, 1668, 1591, 1449, 1356, 1249, 1166, 1063; ^{1}H NMR (400 MHz, $CDCl_3$, δ/ppm): 1.75-1.81 (br, s, 4H, alkyl (-CH_2-)$_4$, *J*=24), 2.69-2.75 (br, s, 4H, alkyl (-CH_2-)$_4$, *J*=24), 3.85 (s, 6H, -CH_3-, *J*=4), 6.99 (d, 4H, Ar, *J*=4), 7.32 (t, 2H, Ar), 7.48 (t, 6H, Ar, *J*=16), 7.64 (d, 4H, Ar, *J*=4), 7.78 (d, 4H, Ar, *J*=8), 8.01 (s, 2H, Ar); ^{13}C NMR (100 MHz, $CDCl_3$, δ/ppm): 204.28, 159.92, 153.99, 139.79, 139.44, 129.89, 129.61, 126.91, 126.56, 126.50, 125.07, 119.41, 119.36, 116.46, 114.21, 55.44, 43.52, 31.39, 29.38, 28.59, 25.39; HR-MS *m*/*z*: [$C_{41}H_{36}N_4O_3$]$^+$, 633.3198 (calc. 632.7495).

(2*E*,7*E*)-2,7-bis((1-phenyl-3-(p-tolyl)-1*H*-pyrazol-4-yl)methylene)cycloheptan-1-one (5m) Yield 63%; m.p.136-141°C; IR (KBr) νmax/cm^{-1}:3062, 2917, 1671, 1592, 1506, 1439, 1339, 1236, 1165, 1067 ; ^{1}H NMR (400 MHz, $CDCl_3$, δ/ppm): 1.74-1.80 (m, 4H, alkyl (-CH_2-)$_4$), 2.39 (s, 6H, -CH_3-), 2.68-2.73 (m, 4H, alkyl (-CH_2-)$_4$), 7.26 (d, 4H, Ar, *J*=12), 7.31 (t, 2H, Ar, *J*=12), 7.47 (t, 6H, Ar, *J*=16), 7.59 (d, 4H, Ar, *J*=8), 7.77 (d, 4H, Ar, *J*=8), 8.00 (s, 2H,Ar); ^{13}C NMR (100 MHz, $CDCl_3$, δ/ppm): 204.25, 154.25, 139.79, 139.47, 138.36, 129.61, 129.46, 128.52, 126.60, 119.39, 116.64, 43.51, 31.39, 29.37, 28.60, 25.39, 21.47; HR-MS *m*/*z*: [$C_{41}H_{36}N_4O$]$^+$, 601.2966 (calc. 600.7507).

(2*E*,7*E*)-2,7-bis((3-(4-nitrophenyl)-1-phenyl-1*H*-pyrazol-4-yl)methylene)cycloheptan-1-one (5n)Yield 82 %; m.p. 132-137°C; IR (KBr) νmax/cm^{-1}: 3051, 2928, 1680, 1597, 1537, 1338, 1226, 1166, 1089; ^{1}H NMR (400 MHz, $CDCl_3$, δ/ppm): 1.75-1.82 (m, 4H, alkyl (-CH_2-)$_4$), 2.65-2.72 (m, 4H, alkyl (-CH_2-)$_4$), 7.33-7.51 (m, 12H, Ar), 7.64 (t, 4H, Ar, *J*=12), 7.75 (t, 4H, Ar, *J*=20), 8.00 (s, 2H, Ar); ^{13}C NMR (100 MHz, $CDCl_3$, δ/ppm): 204.15, 197.36, 162.64, 153.22, 152.79, 140.06, 139.62, 130.116, 129.81, 129.67, 129.01, 128.96, 127.19, 126.82, 125.81, 119.48, 119.41, 43.49, 36.60, 31.92, 31.52, 31.35, 29.41, 29.22, 28.57, 28.38, 26.71, 25.40; HR-MS *m*/*z*: [$C_{39}H_{30}N_6O_5$]$^+$, 663.2353 (calc. 662.6927)

(2*E*,7*E*)-2,7-bis((3-(4-chlorophenyl)-1-phenyl-1*H*-pyrazol-4-yl)methylene)cycloheptan-1-one (5o)Yield 37 %; m.p. 265-271°C; IR (KBr) νmax/cm^{-1}: 3069, 2938, 1661, 1597, 1227, 1183, 1065; ^{1}H NMR (400 MHz, $CDCl_3$, δ/ppm): 1.98 (s, 4H, alkyl (-CH_2-)$_4$), 2.70-2.75 (m, 4H, alkyl (-CH_2-)$_4$), 7.36-7.41 (m, 4H, Ar), 7.49-7.54 (m, 4H, Ar), 7.78 (t, 4H, Ar, *J*=20), 7.92 (t, 4H, Ar, *J*=16), 8.15 (s, 2H, Ar), 8.30-8.35 (m, 4H, Ar); ^{13}C NMR (100 MHz, DMSO- d_6, δ/ppm): 203.61, 150.88, 147.65, 141.61, 139.47, 139.21, 130.17, 129.90, 129.55, 129.13, 127.86, 124.62, 124.25, 119.74, 117.11, 43.26, 30.98, 29.42, 28.11, 26.81, 26.29, 25.41; HR-MS *m*/*z*: [$C_{39}H_{30}Cl_2N_4O$]$^+$, 641.1877 (calc. 641.5877)

A flowchart summarizing the development and evaluation phases of the curcuminoids is provided below in Figure 6 to offer a clear and concise overview of the experimental approach.

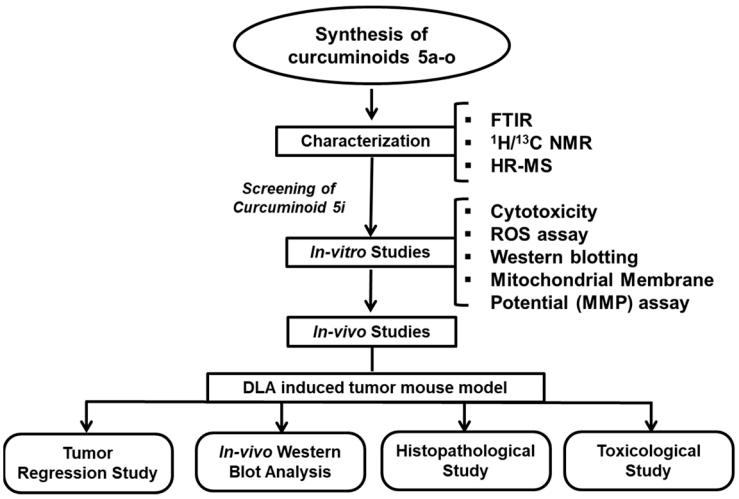

Figure 6. Flowchart summarizing the experimental approach.

4.2. In Vitro Studies

4.2.1. Cell Lines and Cultures

 doi:10.20944/preprints202501.1735.v1

MOLT-4 and HEK-293 cells were obtained from NCCS, Pune. RPMI-1640 was used to culture MOLT-4 cells, whereas HEK-293 cells were cultured in DMEM. All mediums were supplemented with 10% FBS and 1X antimycotic-antibiotic components. Cultures are kept at 37°C with 5% CO_2 in an incubator.

4.2.2. MTT Assay

10000 cells per well of MOLT-4 and HEK-293 were seeded in a 96-well plate. Cells were exposed to the indicated concentrations of drugs (0.01 μM - 10 mM) for 48 h. After treatment, 5 μl of MTT (5 mg/mL) reagent was added to each well and incubated at 37°C for color development. The reaction was then stopped by adding N,N-Dimethylformamide at 50% concentration plus 10% SDS. Cell viability was plotted as a bar graph using the absorbance measured at 570 nm with the spectramax i3X microplate reader [46].

4.2.3. Resazurin Assay

MOLT-4 cells were seeded in a 96-well plate at 10,000 cells per well. The cells were treated for 48 h with different concentrations of the drug ranging from 0.1 μM to 10 mM. Resazurin was added after treatment to all wells at a final concentration of 22 μM and incubated until the color changed from blue to pink. The fluorescence produced was measured using a microplate reader at the excitation wavelength of 550 nm and emission wavelength of 590 nm. Cell viability was represented by a bar graph plotted against the fluorescence produced.

4.2.4. JC-1 Mitochondrial Membrane Potential (ΔΨm) Assay

The kit for mitochondrial membrane potential from Elaboscience was used. MOLT-4 cells were seeded at 100,000 cells/mL in a 12-well plate and treated with 5i for 48 h. The cells were collected, then resuspended in JC-1 dye after incubating at 37°C in the dark. Cells were then transferred to ice-cold JC-1 buffer and analyzed. Flow cytometry (Gallios, Beckman Coulter) acquired 10,000 events, and scatter plot represented mitochondrial potential using the built-in Gallios software.

4.2.5. Western Blotting

5i treated and control cells were harvested and lysed in RIPA buffer (1M tris pH-8, 1% triton-x-100, 0.5% sodium deoxycholate, 1% sodium chloride, 0.1% SDS, 1 mM sodium orthovanadate) supplemented with protease inhibitory cocktail from MP Biomedicals. Total protein concentration was determined by the Bradford method and resolved 35 μg of protein in SDS-PAGE which was then transferred to PVDF membrane. The membrane was cut and probed with the appropriate antibodies. The concentrations for the antibodies were Bcl-2 (Cloud Clone corp) at 1:1000, Bax (Cloud Clone corp) at 1:1000, Bak (CST) at 1:1000, Cytochrome C (CST) at 1:500, Cleaved Caspase 3 (CST) at 1:1000, GAPDH (Cloud Clone corp) at 1:8000, β-actin (Cloud Clone corp) at 1:8000, Anti-rabbit IgG-HRP (CST) at 1:1000 and Anti-mouse IgG-HRP (CST) at 1:1000. Protein bands were visualized using the enhanced chemiluminescence substrate from Bio-Rad and images captured on the Bio-Rad Gel doc system. ImageJ was used to quantify the protein band intensities.

4.3. In Vivo Studies

4.3.1. Animals

Mice were handled and tested following the guidelines set forth by the IBAB Animal Ethics Committee and the Indian national regulations regarding the care and use of animals. The Institutional Ethics Committee of IBAB, Bangalore, India (Ref. IAEC/IBAB/232024), approved the animal experiments conducted for this study, which also adhered to the ARRIVE guidelines. Female Swiss albino mice of 6–8 weeks age (body weight 19–22 g) were procured from Liveon Biolabs Pvt. Ltd., Bangalore, India. The mice were kept in rooms with controlled humidity, temperature (23 ±

 doi:10.20944/preprints202501.1735.v1

3°C), and light cycle (12 h dark/12 h light). Ventilated polypropylene cages housed the animals that had a standard pellet diet provided by Liveon Biolabs Pvt. Ltd. The standard pellet diet constituted 21% protein, 5% lipids, 4% crude fiber, 8% ash, 1% calcium, 6% phosphorus, 3.4% glucose, 2% vitamins, and 55% nitrogen-free extract (carbohydrates).

4.3.2. Investigating the Anticancer Potential of 5i in Mice Models

This study was conducted using models of Dalton's Lymphoma Ascites (DLA). For the induction of the tumor, 0.5 million cells were injected in the left thigh of mice. The animals were divided into two groups: Control group n = 5; treated group n = 5. Measurements were recorded on day seven post-tumor implantation using vernier calipers. Group II (treated) animals received intraperitoneal injections of 50 mg/kg body weight of 5i daily throughout the study period. Preliminary studies determined the dosage. Animal body weights were recorded, and daily measurements of tumor size were taken using vernier calipers. The formula V= (ab2)/2 was used to calculate volume, where "a" and "b" represent major and minor diameters, respectively. Animals were sacrificed at the end of the experimental period, and organs including tumors extracted for staining and protein extraction.

4.3.3. Histological Evaluation of Tumor and Organs (Hematoxylin and Eosin Staining)

The tissues were fixed, processed and paraffin embedded following the standard procedure. Sections of 5 μm thickness were cut using a rotary microtome (Leica Biosystems, Wetzlar, Germany) and stained with Hematoxylin and Eosin as required. Stained sections were microscopically examined and images at an appropriate magnification were obtained [47].

Statistical analysis: Statistical analysis was conducted using GraphPad Prism version 8.4.2. The significance between the treatment and its paired control was determined by a student t-test or one-way ANOVA followed by Tukey's multiple comparisons. All data are presented as mean ± standard deviation (SD). The obtained p values were plotted and designated as * ($p \leq 0.05$), ** ($p \leq 0.01$), *** ($p \leq 0.001$), **** ($p \leq 0.0001$) and ns as not significant.

5. Conclusions

A set of curcuminoids (5a-o) was prepared in satisfactory yields, fully characterized and evaluated for cytotoxicity. Of these, we report for the first time a newcompound, (2*E*,5*E*)-2,5-bis((3-(4-nitrophenyl)-1-phenyl-1*H*-pyrazol-4-yl)methylene)cyclopentane-1-one (5i), which exhibits significantly enhanced anticancer activity against leukemia and lymphoma compared to its parent compound, curcumin. Our results reveal that 5i effectively activates intrinsic apoptosis, which subsequently mediates the inhibition of cell proliferation in both in vitro and in vivo conditions. Moreover, 5i remarkably inhibits tumor growth with minimal systemic toxicity at low doses; thus, making it a promising therapeutic candidate.

Supplementary Materials: The following are available online at www.mdpi.com/xxx/s1

Author Contributions: Conceptualization, SSK and BC.; methodology, VS and SP; software, FR; validation, VS, SP and FR; formal analysis, VS, SP, BC and SSK; investigation, VS, SK and SP; resources, VS and SP; data curation, VS, and FR; writing—original draft preparation, VS, SSK and BC; writing—review and editing, VS, SSK and BC; visualization, VS, BC and SSK; supervision, SSK and BC; project administration, SSK and BC. All authors have read and agreed to the published version of the manuscript.

Funding: The APC was funded by KAHER-Belagavi.

Institutional Review Board Statement: The study was conducted according Institutional Ethics Committee of Institute of Bioinformatics and Biotechnology (Ref. IAEC/IBAB/232024).

Acknowledgments: The authors thank the management of the KLE College of Pharmacy (A constituent unit of KAHER-Belagavi), Rajajinagar, Bengaluru 560010 Karnataka, India for providing all the research facilities required.

Conflicts of Interest: The authors declare no conflict of interest.

References

1. Fah Chueahongthong; Tima, S.; Sawitree Chiampanichayakul; Berkland, C.; Songyot Anuchapreeda The Effect of Co-Treatments of Chemotherapeutic Drugs and Curcumin on Cytotoxicity and FLT3 Protein Expression in Leukemic Stem Cells. Research Square (Research Square) 2021, doi:https://doi.org/10.21203/rs.3.rs-467881/v1.
2. Major Cancer Types by Deaths Worldwide 2020 Available online: https://www.statista.com/statistics/288580/number-of-cancer-deaths-worldwide-by-type/(accessed on 18 May 2024).
3. GUNZ, F.W.; HOUGH, R.F. Acute Leukemia over the Age of Fifty: A Study of Its Incidence and Natural History. Blood 1956, 11, 882–901, doi:https://doi.org/10.1182/blood.v11.10.882.882.
4. Tebbi, C.K. Etiology of Acute Leukemia: A Review. Cancers 2021, 13, 2256, doi:https://doi.org/10.3390/cancers13092256.
5. Burcu Güleryüz; Ayşe Işık; Murat Gülsoy Synergistic Effect of Mesoporous Silica Nanocarrier-Assisted Photodynamic Therapy and Anticancer Agent Activity on Lung Cancer Cells. Lasers in Medical Science 2024, 39, doi:https://doi.org/10.1007/s10103-023-03969-x.
6. Othman, E.M.; Fayed, E.A.; Husseiny, E.M.; Abulkhair, H.S. Apoptosis Induction, PARP-1 Inhibition, and Cell Cycle Analysis of Leukemia Cancer Cells Treated with Novel Synthetic 1,2,3-Triazole-Chalcone Conjugates. Bioorganic Chemistry 2022, 123, 105762, doi:https://doi.org/10.1016/j.bioorg.2022.105762.
7. Mazumder, K.; Aktar, A.; Roy, P.; Biswas, B.; Hossain, Md.E.; Sarkar, K.K.; Bachar, S.C.; Ahmed, F.; Monjur-Al-Hossain, A.S.M.; Fukase, K. A Review on Mechanistic Insight of Plant Derived Anticancer Bioactive Phytocompounds and Their Structure Activity Relationship. Molecules 2022, 27, 3036, doi:https://doi.org/10.3390/molecules27093036.
8. Kunnumakkara, A.B.; Hegde, M.; Dey Parama; Sosmitha Girisa; Kumar, A.; Uzini Devi Daimary; Prachi Garodia; Sarat Chandra Yenisetti; Oommen, O.V.; Aggarwal, B.B. Role of Turmeric and Curcumin in Prevention and Treatment of Chronic Diseases: Lessons Learned from Clinical Trials. ACS Pharmacology & Translational Science 2023, 6, 447–518, doi:https://doi.org/10.1021/acsptsci.2c00012.
9. Jacob, S.; Kather, F.; Morsy, M.; Sai Boddu; Mahesh Attimarad; Shah, J.; Pottathil Shinu; Nair, A. Advances in Nanocarrier Systems for Overcoming Formulation Challenges of Curcumin: Current Insights. Nanomaterials 2024, 14, 672–672, doi:https://doi.org/10.3390/nano14080672.
10. Wilken, R.; Veena, M.S.; Wang, M.B.; Srivatsan, E.S. Curcumin: A Review of Anti-Cancer Properties and Therapeutic Activity in Head and Neck Squamous Cell Carcinoma. Molecular Cancer 2011, 10, 12, doi:https://doi.org/10.1186/1476-4598-10-12.
11. Nishimura, F.G.; Sampaio, B.B.; Oliveira, G.; Silva; Julia; Kamila Chagas Peronni; Evangelista, A.F.; Hossain, M.; Dimmock, J.R.; Bandy, B.; et al. The Transcriptome of BT-20 Breast Cancer Cells Exposed to Curcumin Analog NC2603 Reveals a Relationship between EGR3 Gene Modulation and Cell Migration Inhibition. Molecules 2024, 29, 1366–1366, doi:https://doi.org/10.3390/molecules29061366.
12. MaruYama, T.; Hiroyuki Yamakoshi; Iwabuchi, Y.; Shibata, H. Mono-Carbonyl Curcumin Analogs for Cancer Therapy. Biological & pharmaceutical bulletin 2023, 46, 756–763, doi:https://doi.org/10.1248/bpb.b23-00103.
13. Srivastava, S.; Mishra, S.; Surolia, A.; Panda, D. C1, a Highly Potent Novel Curcumin Derivative, Binds to Tubulin, Disrupts Microtubule Network and Induces Apoptosis. Bioscience Reports 2016, 36, doi:https://doi.org/10.1042/bsr20160039.
14. Kaur, K.; Al-Khazaleh, A.K.; Bhuyan, D.J.; Li, F.; Li, C.G. A Review of Recent Curcumin Analogues and Their Antioxidant, Anti-Inflammatory and Anticancer Activities. Antioxidants 2024, 13, doi:https://doi.org/10.20944/preprints202403.1292.v1.
15. Jha, N.S.; Mishra, S.; Jha, S.K.; Surolia, A. Antioxidant Activity and Electrochemical Elucidation of the Enigmatic Redox Behavior of Curcumin and Its Structurally Modified Analogues. Electrochimica Acta 2015, 151, 574–583, doi:https://doi.org/10.1016/j.electacta.2014.11.026.

16. Chakraborti, S.; Dhar, G.; Dwivedi, V.; Das, A.; Poddar, A.; Chakraborti, G.; Basu, G.; Chakrabarti, P.; Surolia, A.; Bhattacharyya, B. Stable and Potent Analogues Derived from the Modification of the Dicarbonyl Moiety of Curcumin. Biochemistry 2013, 52, 7449–7460, doi:https://doi.org/10.1021/bi400734e.
17. Marchiani, A.; Rozzo, C.; Fadda, A.; Delogu, G.; Ruzza, P. Curcumin and Curcumin-like Molecules: From Spice to Drugs. Current Medicinal Chemistry 2013, 21, 204–222, doi:https://doi.org/10.2174/092986732102131206115810.
18. Xu, F.; Chen, M.; Chen, H.; Wu, N.; Qi, Q.; Jiang, X.; Fang, D.; Feng, Q.; Jin, R.; Jiang, L. The Curcumin Analog Da0324 Inhibits the Proliferation of Gastric Cancer Cells Via HOTAIRM1/MiR-29b-1-5p/PHLPP1 Axis. Journal of Cancer 2022, 13, 2644–2655, doi:https://doi.org/10.7150/jca.69970.
19. Liang, G.; Shao, L.; Wang, Y.; Zhao, C.; Chu, Y.; Xiao, J.; Zhao, Y.; Li, X.; Yang, S. Exploration and Synthesis of Curcumin Analogues with Improved Structural Stability Both in Vitro and in Vivo as Cytotoxic Agents. Bioorganic & Medicinal Chemistry 2009, 17, 2623–2631, doi:https://doi.org/10.1016/j.bmc.2008.10.044.
20. Reddy, R.; E. Shivakumar; Ramachandran, D. Design, Synthesis and Anticancer Evaluation of Substituted Aryl-1,3-Oxazole Incorporated Pyrazole-Thiazole Derivatives as Anticancer Agents. Chemical Data Collections 2024, 51, 101127–101127, doi:https://doi.org/10.1016/j.cdc.2024.101127.
21. Perugu Edukondalu; Reddymasu Sireesha; Pushpalatha Kavuluri; Suresh, P.; Rao, C.; Chandrasekhar, C.; Rudraraju Ramesh Raju Design, Synthesis and Biological Evaluation of Sulfonamide Derivatives of Benzothiazol-Quinoline-Pyrazoles as Anticancer Agents. Chemical Data Collections 2024, 101136–101136, doi:https://doi.org/10.1016/j.cdc.2024.101136.
22. Lusardi, M.; Signorello, M.G.; Russo, E.; Caviglia, D.; Ponassi, M.; Iervasi, E.; Rosano, C.; Chiara Brullo; Spallarossa, A. Structure–Activity Relationship Studies on Highly Functionalized Pyrazole Hydrazones and Amides as Antiproliferative and Antioxidant Agents. International Journal of Molecular Sciences 2024, 25, 4607–4607, doi:https://doi.org/10.3390/ijms25094607.
23. Boshta, N.M.; Temirak, A.; El-Shahid, Z.A.; Shafiq, Z.; Ahmed A.F. Soliman Design, Synthesis, Molecular Docking and Biological Evaluation of 1,3,5-Trisubstituted-1H-Pyrazole Derivatives as Anticancer Agents with Cell Cycle Arrest, ERK and RIPK3- Kinase Activities. Bioorganic chemistry 2024, 143, 107058–107058, doi:https://doi.org/10.1016/j.bioorg.2023.107058.
24. Kachhot, K.D.; Vaghela, F.H.; Dhamal, C.H.; Vegal, N.K.; Bhatt, T.D.; Joshi, H.S. Water-Promoted Synthesis of Pyrazole-Thiazole-Derivatives as Potent Antioxidants and Their Anti-Cancer Activity: ADMET and SAR Studies. ChemistrySelect 2024, 9, doi:https://doi.org/10.1002/slct.202303521.
25. Zhang, L.; Li, C. Eco-Friendly Green Synthesis of N-Pyrazole Amino Chitosan Using PEG-400 as an Anticancer Agent against Gastric Cancer Cells via Inhibiting EGFR. In Vitro Cellular & Developmental Biology - Animal 2024, 60, 365–373, doi:https://doi.org/10.1007/s11626-024-00890-7.
26. Husseiny, E.M.; Hamada S. Abulkhair; El-Dydamony, N.M.; Anwer, K.E. Exploring the Cytotoxic Effect and CDK-9 Inhibition Potential of Novel Sulfaguanidine-Based Azopyrazolidine-3,5-Diones and 3,5-Diaminoazopyrazoles. Bioorganic Chemistry 2023, 133, 106397–106397, doi:https://doi.org/10.1016/j.bioorg.2023.106397.
27. Malebari, A.M.; E. A. Ahmed, H.; Ihmaid, S.K.; Omar, A.M.; Muhammad, Y.A.; Althagfan, S.S.; Aljuhani, N.; A. A. El-Sayed, A.-A.; Halawa, A.H.; El-Tahir, H.M.; et al. Exploring the Dual Effect of Novel 1,4-Diarylpyranopyrazoles as Antiviral and Anti-Inflammatory for the Management of SARS-CoV-2 and Associated Inflammatory Symptoms. Bioorganic Chemistry 2023, 130, 106255, doi:https://doi.org/10.1016/j.bioorg.2022.106255.
28. Zhou, H.; Ning, Y.; Zeng, G.; Zhou, C.; Ding, X. Curcumin Promotes Cell Cycle Arrest and Apoptosis of Acute Myeloid Leukemia Cells by Inactivating AKT. Oncology Reports 2021, 45, doi:https://doi.org/10.3892/or.2021.7962.
29. Vanneman, M.; Dranoff, G. Combining Immunotherapy and Targeted Therapies in Cancer Treatment. Nature Reviews Cancer 2012, 12, 237–251, doi:https://doi.org/10.1038/nrc3237.
30. Noureddin, S.A.; El-Shishtawy, R.M.; Al-Footy, K.O. Curcumin Analogues and Their Hybrid Molecules as Multifunctional Drugs. European Journal of Medicinal Chemistry 2019, 182, 111631, doi:https://doi.org/10.1016/j.ejmech.2019.111631.

31. Othman, E.M.; Fayed, E.A.; Husseiny, E.M.; Abulkhair, H.S. The Effect of Novel Synthetic Semicarbazone- and Thiosemicarbazone-Linked 1,2,3-Triazoles on the Apoptotic Markers, VEGFR-2, and Cell Cycle of Myeloid Leukemia. Bioorganic chemistry 2022, 127, 105968–105968, doi:https://doi.org/10.1016/j.bioorg.2022.105968.
32. Pandey, M.K.; Kumar, S.; Thimmulappa, R.K.; Parmar, V.S.; Biswal, S.; Watterson, A.C. Design, Synthesis and Evaluation of Novel PEGylated Curcumin Analogs as Potent Nrf2 Activators in Human Bronchial Epithelial Cells. European Journal of Pharmaceutical Sciences 2011, 43, 16–24, doi:https://doi.org/10.1016/j.ejps.2011.03.003.
33. Murwanti, R.; Rahmadani, A.; Ritmaleni, R.; Hermawan, A.; Sudarmanto, B.S.A. Curcumin Analogs Induce Apoptosis and G2/M Arrest in 4T1 Murine Triple-Negative Breast Cancer Cells. Indonesian Journal of Pharmacy 2020, 31, 11, doi:https://doi.org/10.14499/indonesianjpharm31iss1pp11.
34. Yeap, S.K.; Mohd Ali, N.; Akhtar, M.N.; Razak, N.A.; Chong, Z.X.; Ho, W.Y.; Boo, L.; Zareen, S.; Kurniawan, T.A.; Avtar, R.; et al. Induction of Apoptosis and Regulation of MicroRNA Expression by (2E,6E)-2,6-Bis-(4-Hydroxy-3-Methoxybenzylidene)-Cyclohexanone (BHMC) Treatment on MCF-7 Breast Cancer Cells. Molecules 2021, 26, 1277, doi:https://doi.org/10.3390/molecules26051277.
35. Gan, X.; Wu, Y.; Zhu, M.; Liu, B.; Kong, M.; Xi, Z.; Li, K.; Wang, H.; Su, T.; Yao, J.; et al. Design, Synthesis, and Evaluation of Cyclic C7-Bridged Monocarbonyl Curcumin Analogs Containing an O -Methoxy Phenyl Group as Potential Agents against Gastric Cancer. Journal of Enzyme Inhibition and Medicinal Chemistry 2024, 39, doi:https://doi.org/10.1080/14756366.2024.2314233.
36. Wang, L.; Wang, C.; Tao, Z.; Zhao, L.; Zhu, Z.H.; Wu, W.; He, Y.; Chen, H.; Zheng, B.; Huang, X.; et al. Curcumin Derivative WZ35 Inhibits Tumor Cell Growth via ROS-YAP-JNK Signaling Pathway in Breast Cancer. Journal of Experimental & Clinical Cancer Research 2019, 38, doi:https://doi.org/10.1186/s13046-019-1424-4.
37. Xiao, J. A Novel Mono-Carbonyl Analogue of Curcumin Induces Apoptosis in Ovarian Carcinoma Cells via Endoplasmic Reticulum Stress and Reactive Oxygen Species Production. Molecular Medicine Reports 2011, 5, doi:https://doi.org/10.3892/mmr.2011.700.
38. Manohar, S.; Khan, S.I.; Kandi, S.K.; Raj, K.; Sun, G.; Yang, X.; Calderon Molina, A.D.; Ni, N.; Wang, B.; Rawat, D.S. Synthesis, Antimalarial Activity and Cytotoxic Potential of New Monocarbonyl Analogues of Curcumin. Bioorganic & Medicinal Chemistry Letters 2013, 23, 112–116, doi:https://doi.org/10.1016/j.bmcl.2012.11.004.
39. Adams, B.K.; Ferstl, E.M.; Davis, M.C.; Herold, M.; Kurtkaya, S.; Camalier, R.F.; Hollingshead, M.G.; Kaur, G.; Sausville, E.A.; Rickles, F.R.; et al. Synthesis and Biological Evaluation of Novel Curcumin Analogs as Anti-Cancer and Anti-Angiogenesis Agents. Bioorganic & Medicinal Chemistry 2004, 12, 3871–3883, doi:https://doi.org/10.1016/j.bmc.2004.05.006.
40. Wang, J.; Qi, L.; Zheng, S.; Wu, T. Curcumin Induces Apoptosis through the Mitochondria-Mediated Apoptotic Pathway in HT-29 Cells. Journal of Zhejiang University. Science. B 2009, 10, 93–102, doi:https://doi.org/10.1631/jzus.B0820238.
41. Ahmed, M.; Aatif, M.; Ghazala Muteeb; Mir Waqas Alam; Mohamed El Oirdi; Farhan, M. Curcumin and Its Derivatives Induce Apoptosis in Human Cancer Cells by Mobilizing and Redox Cycling Genomic Copper Ions. Molecules 2022, 27, 7410–7410, doi:https://doi.org/10.3390/molecules27217410.
42. Wang, H.; Xu, Y.; Sun, J.; Sui, Z. The Novel Curcumin Derivative 1g Induces Mitochondrial and ER-Stress-Dependent Apoptosis in Colon Cancer Cells by Induction of ROS Production. Frontiers in Oncology 2021, 11, doi:https://doi.org/10.3389/fonc.2021.644197.
43. Bleicken, S.; Classen, M.; Pulagam V. L. Padmavathi; Ishikawa, T.; Zeth, K.; Steinhoff, H.-J.; Enrica Bordignon Molecular Details of Bax Activation, Oligomerization, and Membrane Insertion. Journal of Biological Chemistry 2010, 285, 6636–6647, doi:https://doi.org/10.1074/jbc.m109.081539.
44. Ali, I.; Haque, A.; Saleem, K.; Hsieh, M.F. Curcumin-I Knoevenagel's Condensates and Their Schiff's Bases as Anticancer Agents: Synthesis, Pharmacological and Simulation Studies. Bioorganic & Medicinal Chemistry 2013, 21, 3808–3820, doi:https://doi.org/10.1016/j.bmc.2013.04.018.

 doi:10.20944/preprints202501.1735.v1

45. Vora, J.J.; Vasava, S.B.; Parmar, K.C.; Chauhan, S.; Sharma, S. Synthesis, Spectral and Microbial Studies of Some Novel Schiff Base Derivatives of 4-Methylpyridin-2-Amine. E-journal of Chemistry 2009, 6, 1205–1210, doi:https://doi.org/10.1155/2009/247209.
46. Koroth, J.; Nirgude, S.; Tiwari, S.; Gopalakrishnan, V.; Mahadeva, R.; Kumar, S.; Karki, S.S.; Choudhary, B. Investigation of Anti-Cancer and Migrastatic Properties of Novel Curcumin Derivatives on Breast and Ovarian Cancer Cell Lines. BMC Complementary and Alternative Medicine 2019, 19, doi:https://doi.org/10.1186/s12906-019-2685-3.
47. Murugesan, K.; Koroth, J.; Srinivasan, P.P.; Singh, A.; Mukundan, S.; Karki, S.S.; Choudhary, B.; Gupta, C.M. Effects of Green Synthesised Silver Nanoparticles (ST06-AgNPs) Using Curcumin Derivative (ST06) on Human Cervical Cancer Cells (HeLa) in Vitro and EAC Tumor Bearing Mice Models. International Journal of Nanomedicine 2019, 14, 5257–5270, doi:https://doi.org/10.2147/ijn.s202404.